Journal of Sound and Vibration (2002) **257**(2), 301–319
doi:10.1006/jsvi.5060, available online at http://www.idealibrary.com on IDEAL®

DYNAMIC ANALYSIS OF LARGE-DIAMETER SAGGED CABLES TAKING INTO ACCOUNT FLEXURAL RIGIDITY

Y. Q. Ni

Department of Civil and Structural Engineering, The Hong Kong Polytechnic University, Hung Hom, Kowloon, Hong Kong. E-mail: ceyqni@polyu.edu.hk

J. M. Ko

Faculty of Construction and Land Use, The Hong Kong Polytechnic University, Hung Hom, Kowloon, Hong Kong. E-mail: cejmko@polyu.edu.hk, web http://www.cse.polyu.edu.hk/~dynamics

AND

G. Zheng

Department of Civil and Structural Engineering, The Hong Kong Polytechnic University, Hung Hom, Kowloon, Hong Kong. E-mail: 98902084*r@polyu.edu.hk*

(*Received* 11 *May* 2001, *and in final form* 16 *January* 2002)

For the purpose of developing a vibration-based tension force evaluation procedure for bridge cables using measured multimode frequencies, an investigation on accurate finite element modelling of large-diameter sagged cables taking into account flexural rigidity and sag extensibility is carried out in this paper. A three-node curved isoparametric finite element is formulated for dynamic analysis of bridge stay cables by regarding the cable as a combination of an "ideal cable element" and a fictitious curved beam element in the variational sense. With the developed finite element formulation, parametric studies are conducted to evaluate the relationship between the modal properties and cable parameters lying in a wide range covering most of the cables in existing cable-supported bridges, and the effect of cable bending stiffness and sag on the natural frequencies. A case study is eventually provided to compare the measured natural frequencies of main cables of the Tsing Ma Bridge and the computed frequencies with and without considering cable bending stiffness. The results show that ignoring bending stiffness gives rise to unacceptable errors in predicting higher order natural frequencies of the cables, and the proposed finite element formulation provides an accurate baseline model for cable tension identification from measured multimode frequencies.

1. INTRODUCTION

Advances in modern construction technology have resulted in increasing application of large-diameter and long-span structural cables in cable-supported bridges. As a result of carrying both road and rail traffic, the Tsing Ma Bridge in Hong Kong, a suspension bridge with the main span of 1377 m [1], has the most heavily loaded cables in the world. The main cable section of the bridge is about 1·1 m in diameter after compacting. The Akashi Kaikyo Bridge in Japan, which is the world's longest suspension bridge with the

0022-460X/02/$35.00

main span of 1991 m, also has the main cables of about 1·1 m diameter [2]. The effect of bending stiffness in these large-diameter bridge cables is not negligible. With the Tatara Bridge being a landmark, the construction of cable-stayed bridges is now entering a new era, with main spans reaching 1000 m. The Stonecutters Bridge, currently under design in Hong Kong, is a cable-stayed bridge with the main span of 1018 m [3, 4]. The Tatara Bridge with 890 m main span, which is the existing longest cable-stayed bridge in the world [5], has its longest stay cables of about 460 m in length. A recent design trend for this bridge type is the multi-span cable-stayed bridges with three or more towers [6, 7]. A critical problem of multi-span cable-stayed bridges is the stabilization of the central tower(s), which has resulted in increasing application of extremely long stabilizing cables. For example, the three-tower Ting Kau Bridge in Hong Kong utilizes eight longitudinal stabilizing cables of 465 m long for strengthening the slender central tower [8]. These long stay cables exhibit considerably large sags, and consequently, the effect of sag–extensibility on the cable static and dynamic characteristics is noticeable.

During the construction and service life of a cable-supported bridge, it is essential to accurately define the cable forces, whose change due to degradation or other factors will affect internal force distribution in the deck and towers and influence the bridge alignment. As a result, the cable tension is an important index for assessing overall structural health and condition of cable-supported bridges. Vibration measurement has been one of the most widely used methods for *in situ* evaluation of cable tension forces [9–12]. The engineering implementation of this technique is mostly done based on the taut string theory. According to this theory, cable tension force can be estimated from the measured fundamental natural frequency based on a simple explicit relation. However, recent studies [13–15] indicated that identification based on this simplified formula could not provide accurate tension force estimation for bridge cables in many situations, and showed that cable sag–extensibility and bending rigidity might have pronounced effects on the modal properties and tension force identification of long-span bridge cables. In addition, it has been demonstrated [11, 16] that the identification procedures based on multimode frequencies can provide more accurate cable tension evaluation than the conventional approach using only fundamental natural frequency. This needs a cable model that can accurately predict the relation between the modal properties and cable parameters. The string theory cannot take into account the sag effect [17], and even the modern cable theory does not consider the flexural rigidity [18, 19].

In the present study, an accurate finite element model for structural cables which takes into account flexural rigidity, sag–extensibility and spatial variability of dynamic tension is formulated for the purpose of cable parameter identification from measured modal properties. For the convenience of capturing the effects of sag–extensibility and flexural rigidity, respectively, the formulation is made as a composition of two separable parts: a pure sagged cable without flexural rigidity and a fictitious curved beam element with only flexural rigidity. Parametric studies are conducted to examine the effects of cable bending stiffness and sag–extensibility on modal properties over a wide parameter range, and to compare the results from the proposed formulation and from the literature. A case study is then presented to analyze the modal dynamic behaviors of a real bridge cable with and without considering bending stiffness. The true modal parameters of the cable are obtained by field ambient vibration measurements, and the predicted and measured natural frequencies are compared to verify significant effect of the bending stiffness on higher-mode frequencies and accuracy of the proposed formulation.

2. FORMULATION

2.1. BASIC ASSUMPTIONS

The finite element formulation derived in this section is based on a pure sagged cable element and a fictitious curved beam element. The cable element is characterized by the following idealizations:

1. the cable material is linearly elastic;
2. the cable is perfectly flexible so that it is capable of developing stresses only in the direction normal to the cross-section;
3. the normal stress is uniform over the cross-sectional area;
4. though the displacement may be arbitrarily large, the strain is assumed to be small, which means that the cross-sectional area does not change during deformation; and
5. the radius of the cable curvature is large with regard to its cross-section dimension.

The curved beam element is characterized by the following idealizations:

1. the material is linearly elastic;
2. a plane section originally normal to the neutral axis remains plane after deformation, but does not necessarily remain normal to the neutral axis (Timoshenko beam's assumption); and
3. the curvature radius of the beam is large with regard to its cross-section dimension.

2.2. THREE-NODE CURVED ELEMENT OF SAGGED CABLE

Without losing generality, the cable static equilibrium profile is assumed in the $x-y$ plane as shown in Figure 1. This initial (static) configuration is defined by $x(s)$ and $y(s)$, here s denotes the arc length co-ordinate. Let L, E, A and m be the cable length, modulus of elasticity, cross-sectional area and mass per unit length respectively. In static equilibrium state, the cable is subjected to dead load and the static tension is $H(s)$. Due to the geometric non-linearity of the cable, the static equilibrium configuration of the cable is achieved through a non-linear iteration process by applying the dead load in a stepwise fashion and continuously updating the geometry of the cable (including the tension force). The Newton–Raphson procedure is used to iteratively calculate the dead-load deformed shape with prescribed cable tension if known. The iteration starts from a straight profile

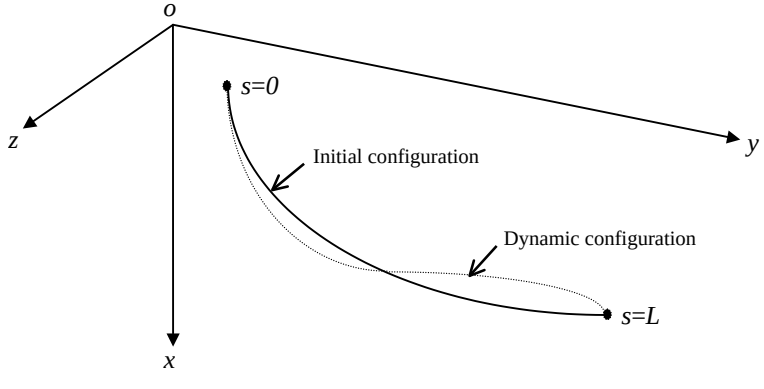

Figure 1. Schematic of cable configuration.

with a presumed tension force. Following this approach, accurate cable profile in static equilibrium state is finally obtained which may be catenary, parabolic or other shapes depending on specific static loads.

After achieving the static equilibrium configuration through a non-linear static analysis, the cable is subjected to the action of dynamic external forces $p_x(s,t), p_y(s,t)$ and $p_z(s,t)$. The dynamic configuration of the cable is described by the displacement responses $u(s,t), v(s,t)$ and $w(s,t)$ measured from the position of static equilibrium in the x, y and z directions respectively. Let $\mathbf{U} = \{u(s,t)\ v(s,t)\ w(s,t)\}^{\mathrm{T}}$ and $\mathbf{P} = \{p_x(s,t)\ p_y(s,t)\ p_z(s,t)\}^{\mathrm{T}}$. By using the Lagrangian strain measure, the cable extensional strain due to dynamic loads, ignoring flexural rigidity, can be expressed as

$$\varepsilon = \varepsilon_0 + \varepsilon_l = \frac{\mathrm{d}\mathbf{X}^{\mathrm{T}}}{\mathrm{d}s}\cdot\frac{\partial\mathbf{U}}{\partial s} + \frac{1}{2}\frac{\partial\mathbf{U}^{\mathrm{T}}}{\partial s}\frac{\partial\mathbf{U}}{\partial s}, \tag{1}$$

where $\mathbf{X} = \{x(s)\ y(s)\ 0\}^{\mathrm{T}}$ is the static equilibrium co-ordinate vector.

The finite element formulation is derived from the Hamilton's principle

$$\delta H = \delta\int_{t_1}^{t_2}\int_0^L (Q - V)\,\mathrm{d}s\,\mathrm{d}t + \int_{t_1}^{t_2}\int_0^L \delta W\,\mathrm{d}s\,\mathrm{d}t = 0 \tag{2}$$

in which Q is the kinetic energy density, V is the elastic strain energy density, and δW is the virtual work density associated with the dead load, dynamic excitation and damping force. They are expressed as

$$Q = \frac{m}{2}\frac{\partial\mathbf{U}^{\mathrm{T}}}{\partial t}\frac{\partial\mathbf{U}}{\partial t}, \tag{3a}$$

$$V = V_i + \frac{EA}{2}\varepsilon^2 + H(s)\varepsilon, \tag{3b}$$

$$\delta W = \delta\mathbf{U}^{\mathrm{T}}\cdot\left(\mathbf{q} + \mathbf{P} - \mathbf{c}\cdot\frac{\partial\mathbf{U}}{\partial t}\right), \tag{3c}$$

where V_i is the elastic strain energy density held in the initial (static) configuration, $\mathbf{q}$ is the dead load vector existent in the initial state and $\mathbf{c} = \mathrm{diag}[c_x\ c_y\ c_z]$ is the viscous damping coefficient matrix.

Substituting equations (3) and (1) into equation (2) yields

$$\begin{aligned}\delta I = \delta\int_{t_1}^{t_2}\int_0^L \Bigg[&\frac{m}{2}\frac{\partial\mathbf{U}^{\mathrm{T}}}{\partial t}\frac{\partial\mathbf{U}}{\partial t} - V_i - \frac{EA}{2}\left(\frac{\mathrm{d}\mathbf{X}^{\mathrm{T}}}{\mathrm{d}s}\frac{\partial\mathbf{U}}{\partial s} + \frac{1}{2}\frac{\partial\mathbf{U}^{\mathrm{T}}}{\partial s}\frac{\partial\mathbf{U}}{\partial s}\right)^2 \\ &- H\left(\frac{\mathrm{d}\mathbf{X}^{\mathrm{T}}}{\mathrm{d}s}\frac{\partial\mathbf{U}}{\partial s} + \frac{1}{2}\frac{\partial\mathbf{U}^{\mathrm{T}}}{\partial s}\frac{\partial\mathbf{U}}{\partial s}\right)\Bigg]\mathrm{d}s\,\mathrm{d}t + \int_{t_1}^{t_2}\int_0^L \delta\mathbf{U}^{\mathrm{T}}\left(\mathbf{q} + \mathbf{P} - \mathbf{c}\frac{\partial\mathbf{U}}{\partial t}\right)\mathrm{d}s\,\mathrm{d}t = 0.\end{aligned} \tag{4}$$

Here the displacement vector $\mathbf{U}$ is selected to fulfill the boundary conditions and initial conditions. By integrating equation (4) by parts and accounting for the static equilibrium configuration, we have

$$\begin{aligned}\delta I = \int_{t_1}^{t_2}\int_0^L \delta\mathbf{U}^{\mathrm{T}}\Bigg\{&m\frac{\partial^2\mathbf{U}}{\partial t^2} - EA\frac{\partial}{\partial s}\left[\left(\frac{\mathrm{d}\mathbf{X}^{\mathrm{T}}}{\mathrm{d}s}\frac{\partial\mathbf{U}}{\partial s} + \frac{1}{2}\frac{\partial\mathbf{U}^{\mathrm{T}}}{\partial s}\frac{\partial\mathbf{U}}{\partial s}\right)\left(\frac{\mathrm{d}\mathbf{X}}{\mathrm{d}s} + \frac{\partial\mathbf{U}}{\partial s}\right)\right] \\ &- \frac{\partial}{\partial s}\left(H\frac{\partial\mathbf{U}}{\partial s}\right) + \mathbf{c}\frac{\partial\mathbf{U}}{\partial t} - \mathbf{P}\Bigg\}\mathrm{d}s\,\mathrm{d}t = 0.\end{aligned} \tag{5}$$

An isoparametric curved element with three nodes is introduced to describe the cable. As shown in Figure 2, the shape functions in the natural co-ordinate system are given by

$$N_1 = \tfrac{1}{2}(1-\xi) - \tfrac{1}{2}(1-\xi^2),\quad N_2 = 1 - \xi^2,\quad N_3 = \tfrac{1}{2}(1+\xi) - \tfrac{1}{2}(1-\xi^2) \tag{6a–c}$$

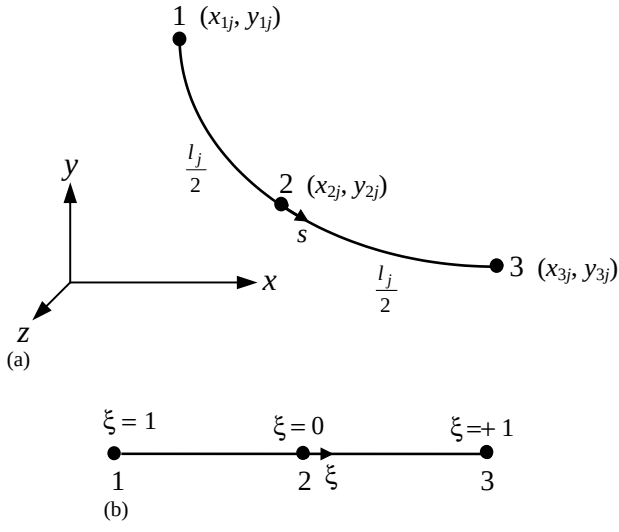

Figure 2. Three-node curved cable element: (a) physical co-ordinate; (b) natural co-ordinate.

and the co-ordinates and the displacement functions are expressed as

$$x = \sum N_i x_i, \quad y = \sum N_i y_i \tag{7a, b}$$

$$u = \sum N_i u_i, \quad v = \sum N_i v_i, \quad w = \sum N_i w_i, \tag{8a – c}$$

where x_i, y_i $(i = 1, 2, 3)$ are the nodal co-ordinates; and the nodal displacement vector is defined as

$$\{\mathbf{U}_j\} = \{\{\mathbf{U}\}_{j1}^{\mathrm{T}} \{\mathbf{U}\}_{j2}^{\mathrm{T}} \{\mathbf{U}\}_{j3}^{\mathrm{T}}\}^{\mathrm{T}} = \{u_{1j}\ v_{1j}\ w_{1j}\ u_{2j}\ v_{2j}\ w_{2j}\ u_{3j}\ v_{3j}\ w_{3j}\}^{\mathrm{T}}. \tag{9}$$

By rewriting equation (8) as

$$\mathbf{U} = \{u\ v\ w\}^{\mathrm{T}} = [N_1\mathbf{I}\ N_2\mathbf{I}\ N_3\mathbf{I}]\{\{\mathbf{U}\}_{j1}^{\mathrm{T}} \{\mathbf{U}\}_{j2}^{\mathrm{T}} \{\mathbf{U}\}_{j3}^{\mathrm{T}}\}^{\mathrm{T}} = [\mathbf{N}]\{\mathbf{U}_j\} \tag{10}$$

and substituting equations (7)–(10) into equation (1), we get the following expressions:

$$\varepsilon_0 = [\mathbf{B}_0]\{\mathbf{U}_j\} = [\{B_{01}\}\ \{B_{02}\}\ \{B_{03}\}]\{\mathbf{U}_j\}, \tag{11a}$$

$$\varepsilon_l = [\mathbf{B}_l]\{\mathbf{U}_j\} = [\{B_{l1}\}\ \{B_{l2}\}\ \{B_{l3}\}]\{\mathbf{U}_j\}, \tag{11b}$$

$$\{B_{0i}\} = \tfrac{1}{J^2}\{x' N_i'\ y' N_i'\ 0\}, \tag{11c}$$

$$\{B_{li}\} = \tfrac{1}{2J^2}\{u' N_i'\ v' N_i'\ w' N_i'\}, \tag{11d}$$

where $J = \mathrm{d}s/\mathrm{d}\xi$ and the prime denotes the derivative with respect to ξ.

Substituting equations (9)–(11) into equation (5), after some manipulation, yields

$$\delta I = \int_{t_1}^{t_2} \sum \delta\{\mathbf{U}_j\}^{\mathrm{T}}\{[\mathbf{M}_j]\{\ddot{\mathbf{U}}_j\} + [\mathbf{C}_j]\{\dot{\mathbf{U}}_j\} + [\mathbf{K}_{0j} + \mathbf{K}_{1j}(\{\mathbf{U}_j\}) + \mathbf{K}_{2j}(\{\mathbf{U}_j\}\{\mathbf{U}_j\}^{\mathrm{T}})]\{\mathbf{U}_j\} - \{\mathbf{P}_j\}\}\,\mathrm{d}t = 0 \tag{12}$$

from which the governing equation of motion of the element j is obtained as

$$[\mathbf{M}_j]\{\ddot{\mathbf{U}}_j\} + [\mathbf{C}_j]\{\dot{\mathbf{U}}_j\} + [\mathbf{K}_{0j} + \mathbf{K}_{1j}(\{\mathbf{U}_j\}) + \mathbf{K}_{2j}(\{\mathbf{U}_j\}\{\mathbf{U}_j\}^{\mathrm{T}})]\{\mathbf{U}_j\} = \{\mathbf{P}_j\} \tag{13}$$

in which

$$[\mathbf{M}_j] = mJ\int_{-1}^{+1}[\mathbf{N}]^{\mathrm{T}}[\mathbf{N}]\,\mathrm{d}\xi, \tag{14a}$$

$$[\mathbf{C}_j] = J\int_{-1}^{+1}[\mathbf{N}]^{\mathrm{T}}[\mathbf{c}][\mathbf{N}]\,\mathrm{d}\xi, \tag{14b}$$

$$\{\mathbf{P}_j\} = J\int_{-1}^{+1}[\mathbf{N}]^{\mathrm{T}}\{\mathbf{P}\}\,\mathrm{d}\xi, \tag{14c}$$

$$[\mathbf{K}_{0j}] = EAJ\int_{-1}^{+1}[\mathbf{B}_0]^{\mathrm{T}}[\mathbf{B}_0]\,\mathrm{d}\xi + \tfrac{1}{2J}\int_{-1}^{+1}H[\mathbf{N}']^{\mathrm{T}}[\mathbf{N}']\,\mathrm{d}\xi, \tag{14d}$$

$$[\mathbf{K}_{1j}] = EAJ\int_{-1}^{+1}([\mathbf{B}_l]^{\mathrm{T}}[\mathbf{B}_0] + 2[\mathbf{B}_0][\mathbf{B}_l])\,\mathrm{d}\xi, \tag{14e}$$

$$[\mathbf{K}_{2j}] = 2EAJ\int_{-1}^{+1}[\mathbf{B}_l]^{\mathrm{T}}[\mathbf{B}_l]\,\mathrm{d}\xi. \tag{14f}$$

The global equation of the cable is then obtained through assembling the element mass matrix, damping matrix, stiffness matrix and nodal load vector by the standard assembly procedure. It is noted that in equation (14) the stiffness matrix includes linear stiffness term $[\mathbf{K}_0]$, quadratically non-linear stiffness term $[\mathbf{K}_1]$ and cubically non-linear stiffness term $[\mathbf{K}_2]$. The present study only addresses linear problem of cable dynamics by ignoring the non-linear stiffness terms. For non-linear dynamic analysis of cables in terms of the above formulae, see reference [20].

2.3. FORMULATION FOR FLEXURAL RIGIDITY

The additional stiffness contribution due to the flexural rigidity of cable is derived by assuming a fictitious curved beam. The curved beam element is same as shown in Figure 2, but a new local co-ordinate system in terms of tangential and normal axes is introduced for the convenience of formulation to relate displacements with stress resultants. As illustrated in Figure 3, the displacements at any node i are expressed as

$$\{\delta\}_i = \{u_i\, v_i\, w_i\, \theta_{si}\, \theta_{ti}\, \theta_{zi}\}^{\mathrm{T}}, \tag{15}$$

where u_i is the in-plane displacement in the tangential direction, v_i is the displacement in the transverse direction, w_i is the displacement in the z direction, θ_{si} is the total rotation in the tangential direction, θ_{ti} is the angle of twist, and θ_{zi} is the total rotation of transverse bending. Similar to equation (9), the displacement vector is expressed with isoparametric interpolation functions as

$$\{\mathbf{U}\} = \{u\, v\, w\, \theta_s\, \theta_t\, \theta_z\}^{\mathrm{T}} = [N_1\mathbf{I}\ N_2\mathbf{I}\ N_3\mathbf{I}]\{\{\delta\}_1^{\mathrm{T}}\ \{\delta\}_2^{\mathrm{T}}\ \{\delta\}_3^{\mathrm{T}}\}^{\mathrm{T}} = [\mathbf{N}]\{\delta\}. \tag{16}$$

The strain vector is written as

$$\{\varepsilon\} = \{\kappa_z\, \kappa_t\, \alpha\, \gamma_{vs}\, \gamma_{ws}\}, \tag{17}$$

where κ_z and κ_t are the in-plane and out-of-plane curvature changes, respectively, α is the cross-sectional torsion change, γ_{vs} and γ_{ws} are the shear strains. The strain–displacement

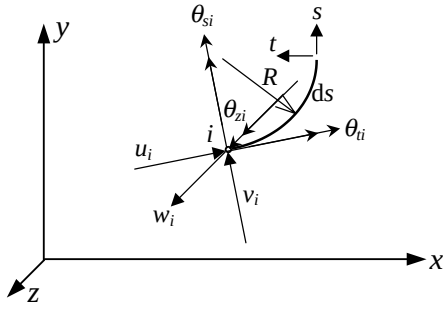

Figure 3. Displacements at node i.

relation can be expressed as

$$\kappa_z = \frac{\partial \theta_z}{\partial s} + \frac{1}{R}\frac{\partial u}{\partial s}, \quad \kappa_t = -\frac{\partial \theta_s}{\partial s} - \frac{\theta_t}{R}, \tag{18a, b}$$

$$\alpha = \frac{\partial \theta_t}{\partial s} - \frac{\theta_s}{R}, \quad \gamma_{vs} = \frac{\partial v}{\partial s} - \theta_z, \quad \gamma_{ws} = \frac{\partial w}{\partial s} + \theta_s \tag{18c–e}$$

in which R is the curvature radius of the element. It should be noted that R is not a constant for a sagged cable. It is calculated using the formula

$$R = \frac{[1 + (\mathrm{d}y/\mathrm{d}x)^2]^{3/2}}{\mathrm{d}^2 y/\mathrm{d}^2 x}. \tag{19}$$

Combining equations (16) and (18) yields

$$\{\varepsilon\} = [\mathbf{B}]\{\delta\} = [[B_1]\,[B_2]\,[B_3]]\{\delta\} \tag{20}$$

in which $[B_i]$ $(i = 1, 2, 3)$ is expressed as

$$[B_i] = \frac{1}{RJ}\begin{bmatrix} N_i' & 0 & 0 & 0 & 0 & RN_i' \\ 0 & 0 & 0 & -RN_i' & -JN_i & 0 \\ 0 & 0 & 0 & -JN_i & RN_i' & 0 \\ 0 & RN_i' & 0 & 0 & 0 & -RJN_i \\ 0 & 0 & RN_i' & JRN_i & 0 & 0 \end{bmatrix}. \tag{21}$$

Figure 4 shows the stress resultants at node i. The stress–strain relation is given by

$$\{\sigma\} = \{M_z\ M_t\ T\ V_z\ V_s\}^{\mathrm{T}} = \mathrm{diag}[EI_z\ EI_s\ GJ_s\ \beta GA\ \beta GA]\{\varepsilon\} = [\mathbf{D}]\{\varepsilon\}. \tag{22}$$

With equations (20) and (22), the additional element stiffness matrix due to cable flexural rigidity is derived in a similar way as

$$[\mathbf{K}_a] = J\int_{-1}^{+1} [\mathbf{B}]^{\mathrm{T}}[\mathbf{D}][\mathbf{B}]\,\mathrm{d}\xi. \tag{23}$$

The additional stiffness matrix given in equation (23) is obtained by referring to the local co-ordinate system. It should be transformed into the element stiffness relation in the global x–y–z co-ordinate system before performing assembly to obtain overall stiffness matrix. Likewise, the element stiffness matrix given in equation (14), with 9×9 dimension, only accommodates the translational degrees of freedom. It should be expanded in the assembly process as an 18×18 matrix to cater for the rotation degrees of freedom.

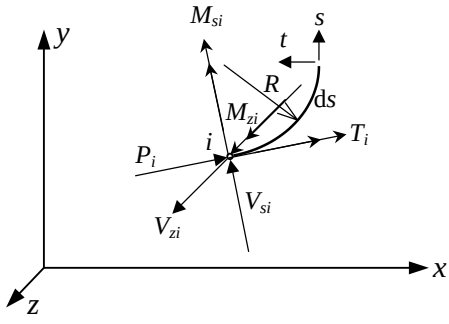

Figure 4. Stress resultants at node *i*.

3. PARAMETRIC STUDIES

The proposed formulation has been encoded into a versatile finite element program. In this section, parametric studies are conducted to evaluate the effect of bending stiffness and sag–extensibility on natural frequencies, and the relation between the modal properties and cable parameters for a wide parameter range. A numerical verification is first carried out by comparing the computed results by the present method with the analytical results available in literature. Mehrabi and Tabatabai [15] formulated a differential equation for solution of free vibration of suspended cables by use of finite difference technique. This approximate formula accounted for cable bending stiffness and sag–extensibility, but was based on the assumption of flat sag and invariability of dynamic tension along cable length. The following dimensionless parameters have been adopted to characterize the bending stiffness and sag–extensibility respectively:

$$\xi = L\sqrt{\frac{H_h}{EI}}, \quad \lambda^2 = \frac{LEA}{H_h L_e}\left(\frac{mgL}{H_h}\right)^2, \tag{24a, b}$$

where H_h is the horizontal component of cable static tension force, I is the moment of inertia of cable cross-section, and

$$L_e = \int_0^L \left(\frac{\mathrm{d}s}{\mathrm{d}x}\right)^3 \mathrm{d}x \cong L\left[1 + \frac{1}{8}\left(\frac{mgL}{H_h}\right)^2\right]. \tag{25}$$

Four suspended cables with the same length of 100 m but different sag–extensibility (λ^2) and bending-stiffness (ξ) parameters are analyzed. Table 1 shows the parameters of the four cables. Cable 1 ($\lambda^2 = 0{\cdot}79, \xi = 605{\cdot}5$) has a moderate sag and a low bending stiffness; Cable 2 ($\lambda^2 = 50{\cdot}70, \xi = 302{\cdot}7$) has a large sag and an average bending stiffness; Cable 3 ($\lambda^2 = 1{\cdot}41, \xi = 50{\cdot}5$) has a moderate sag and a high bending stiffness; Cable 4 ($\lambda^2 = 50{\cdot}70, \xi = 50{\cdot}5$) has a large sag and a high bending stiffness. Modal properties of the four cables are evaluated by the proposed finite element formulation. The static profiles of the cables are assumed as parabolas. Sixty equi-length cable elements are used in the computation. Table 2 presents a comparison of predicted natural frequencies of the first two in-plane modes obtained by the taut string theory, the finite difference formula and the present method. It is observed that for all the four cases the results by the present method coincide well with those by the finite difference formula. Both the methods take into account sag–extensibility and bending stiffness. It is found from the table that the computed natural frequencies from the taut string equation (ignoring sag–extensibility and bending stiffness) are quite different from those calculated by the present method and the

TABLE 1

Material and geometric parameters of four cables

Cable no.	λ^2	ξ	m (kg/m)	g (N/kg)	L (m)	H_h (10^6 N)	E (Pa)	A (m^2)	J_s (m^4)
1	0·79	605·5	400·0	9·8	100·0	2·90360	1·5988e+10	7·8507e−03	4·9535e−06
2	50·70	302·7	400·0	9·8	100·0	0·72590	1·7186e+10	7·6110e−03	4·6097e−06
3	1·41	50·5	400·0	9·8	100·0	26·13254	2·0826e+13	7·8633e−03	4·9204e−06
4	50·70	50·5	400·0	9·8	100·0	0·72590	4·7834e+08	2·7345e−01	5·9506e−03

TABLE 2

Comparison of computed frequencies of in-plane modes (Hz)

Cable no.	λ^2	ξ	String theory		Finite difference formula		Present method	
			First mode	Second mode	First mode	Second mode	First mode	Second mode
1	0·79	605·5	0·426	0·852	0·440	0·853	0·441	0·854
2	50·70	302·7	0·213	0·426	0·428	0·464	0·421	0·460
3	1·41	50·5	1·278	2·556	1·399	2·679	1·400	2·682
4	50·70	50·5	0·213	0·426	0·447	0·464	0·438	0·461

TABLE 3

Parameters of two sets of cables

	Cable set 1				Cable set 2			
	A (m^2)	H_h (N)	d/L	f_{1s} (Hz)	A (m^2)	H_h (N)	d/L	f_{1s} (Hz)
Minimum value	$9{\cdot}788\times10^{-7}$	0·1031	1/23 750	0·5810	$9{\cdot}575\times10^{-5}$	$9{\cdot}846\times10^{2}$	1/2375	0·1817
Maximum value	0·14258	$3{\cdot}236\times10^{6}$	1/110	8·5284	14·258	$3{\cdot}236\times10^{10}$	1/11	2·6969

finite difference formula, indicating a considerable influence of sag–extensibility and bending stiffness in these cases.

In order to relate the modal properties with cable parameters, the relation surfaces of dimensionless frequencies versus λ^2 and ξ are obtained for a wide range of structural parameters. Two cable sets are considered. The fixed cable parameters are $L = 100$ m and $E = 200$ GPa.The change ranges of other parameters are given in Table 3 that result in $0{\cdot}001 \leqslant \lambda^2 \leqslant 10\,000$ and $10 \leqslant \xi \leqslant 260$ for both cable sets. The volume mass density of set 1 is kept as a constant value of $\rho = m/A = 7{\cdot}86\times10^3$ kg/m^3, while the density of set 2 is appropriately altered to produce same ranges of λ^2 and ξ for sets 2 and 1. The main difference between the two sets is the range of their sag-to-span ratio d/L. Both the finite difference formula and the present method are used to compute the relation surfaces. The cable is divided into 50 elements in the finite element solution and 100 elements in the finite difference formula, with totally 101 nodes used for each method. With the computed natural frequency f_n of the nth mode, the corresponding dimensionless frequency is defined as

$$\bar{f}_n = \frac{f_n}{f_{1s}}, \tag{26}$$

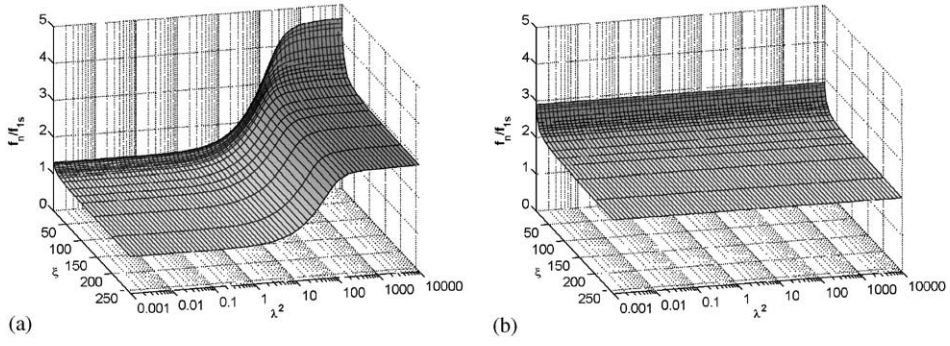

Figure 5. Relation surfaces of two in-plane fundamental modes obtained by finite difference formula: (a) first symmetric mode (cable sets 1 and 2); (b) first antisymmetric mode (cable sets 1 and 2).

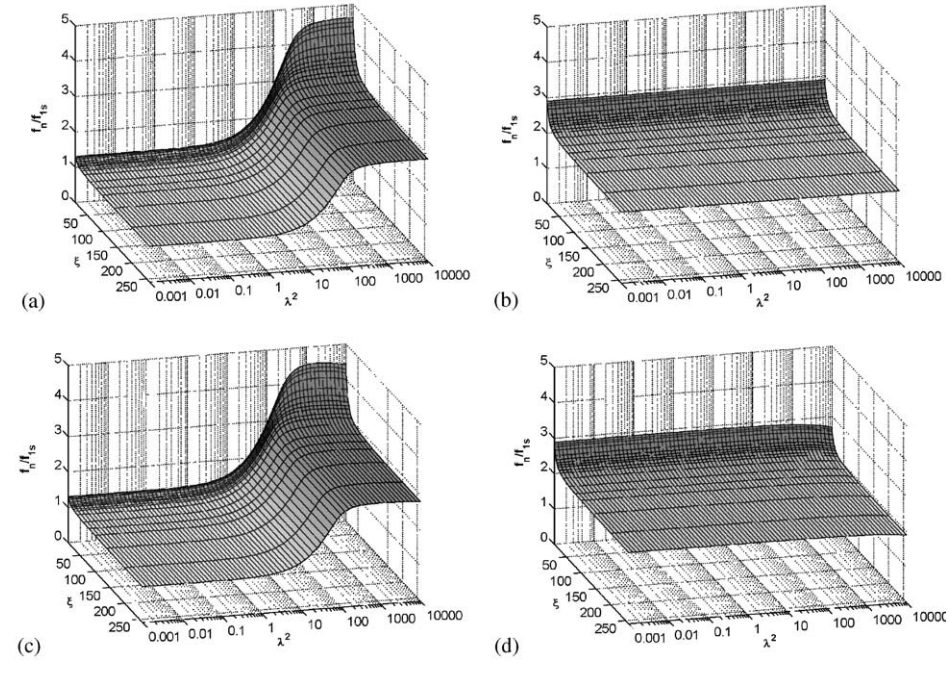

Figure 6. Relation surfaces of two in-plane fundamental modes obtained by the present method: (a) first symmetric mode (cable set 1); (b) first antisymmetric mode (cable set 1); (c) first symmetric mode (cable set 2); (d) first antisymmetric mode (cable set 2).

where f_{1s} is the fundamental frequency of the corresponding stretched string which is obtained from

$$f_{1s} = \frac{1}{2L}\sqrt{\frac{H_h A}{m}}. \tag{27}$$

Figure 5 shows the relation surfaces of dimensionless frequencies versus λ^2 and ξ for the first symmetric and antisymmetric in-plane modes obtained by the finite difference formula. Figure 6 gives the corresponding relation surfaces obtained by the present

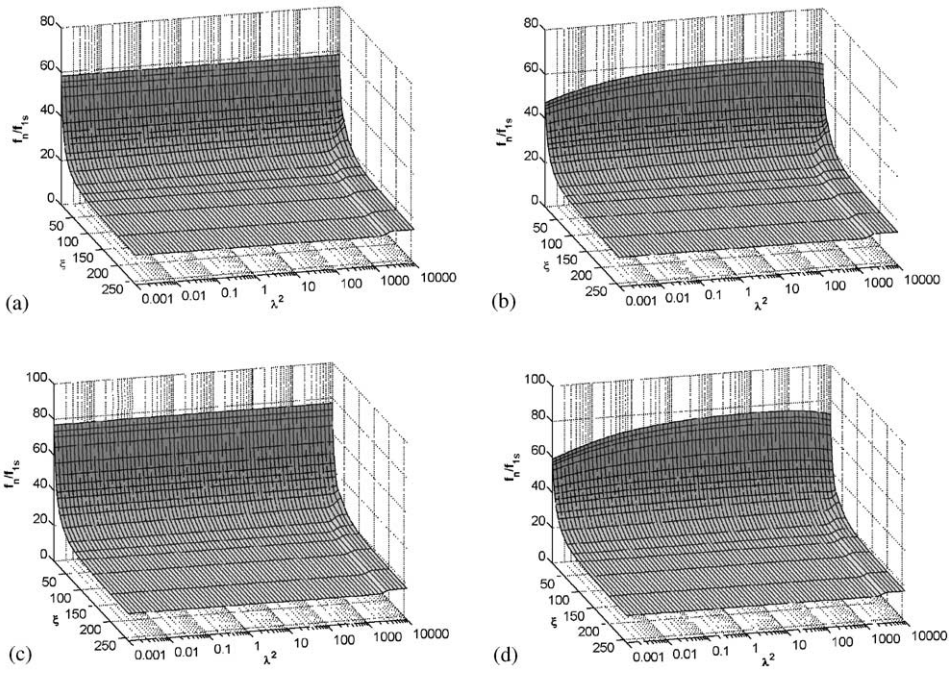

Figure 7. Comparison of relation surfaces of higher order in-plane modes obtained by two methods: (a) seventh symmetric mode by finite difference formula (cable sets 1 and 2); (b) seventh symmetric mode by the present method (cable set 2); (c) eighth symmetric mode by finite difference formula (cable sets 1 and 2); (d) eighth symmetric mode by the present method (cable set 2).

method. By comparing the two figures, it is seen that the results for the two fundamental modes obtained by the approximate finite difference formula and by the present method coincide very well with each other throughout the concerned ranges of λ^2 and ξ for cable set 1 (with low sag-to-span ratio). For cable set 2 (with high sag-to-span ratio), a good agreement is still achieved except for a small region with very high λ^2 and very low ξ where the relation surfaces display a slight difference with each other. Figure 7 provides a comparison of the relation surfaces of two high order modes obtained by the two methods. It is observed that in these cases the results deviate significantly from each other in the range with small ξ. The deviation of the approximate finite difference formula from the finite element results increases with the mode order. Figure 8 illustrates the relation surfaces of dimensionless frequency versus λ^2 and ξ for high order in-plane modes of cable set 2 obtained by the present method. Figure 9 shows the relation surfaces for out-of-plane modes of cable set 2 using the present method. It is obvious from Figures 8 and 9 that the high order frequencies of the in-plane as well as out-of-plane modes depend on both parameters λ^2 and ξ, although the change rate of the frequencies along the parametric axis of λ^2 is much smaller than that along the parametric axis of ξ. This observation is different from that made in reference [15]. These differences are attributed to the fact that the finite difference formula was derived on the assumptions of parabolic static profile, flat sag and spatial invariability of dynamic tension, while the present method eschews these assumptions. The above studies conclude that when high order modal properties are required in an inverse problem, a precise finite element model is more acceptable in regard to its accuracy, versatility and reliability.

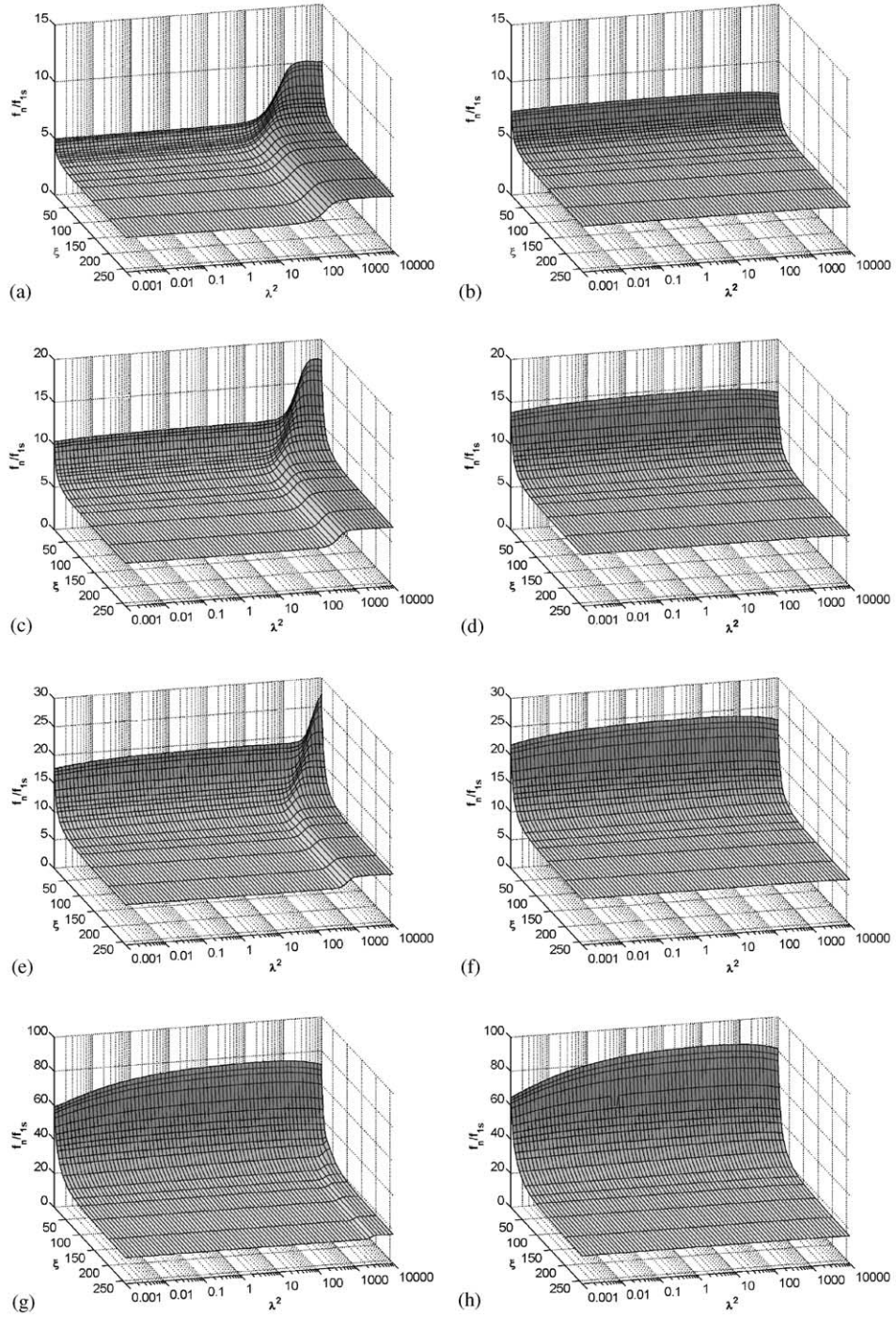

Figure 8. Relation surfaces of high order in-plane modes obtained by the present method for cable set 2: (a) second symmetric mode; (b) second antisymmetric mode; (c) third symmetric mode; (d) third antisymmetric mode; (e) fourth symmetric mode; (f) fourth antisymmetric mode; (g) eighth symmetric mode; (h) eighth antisymmetric mode.

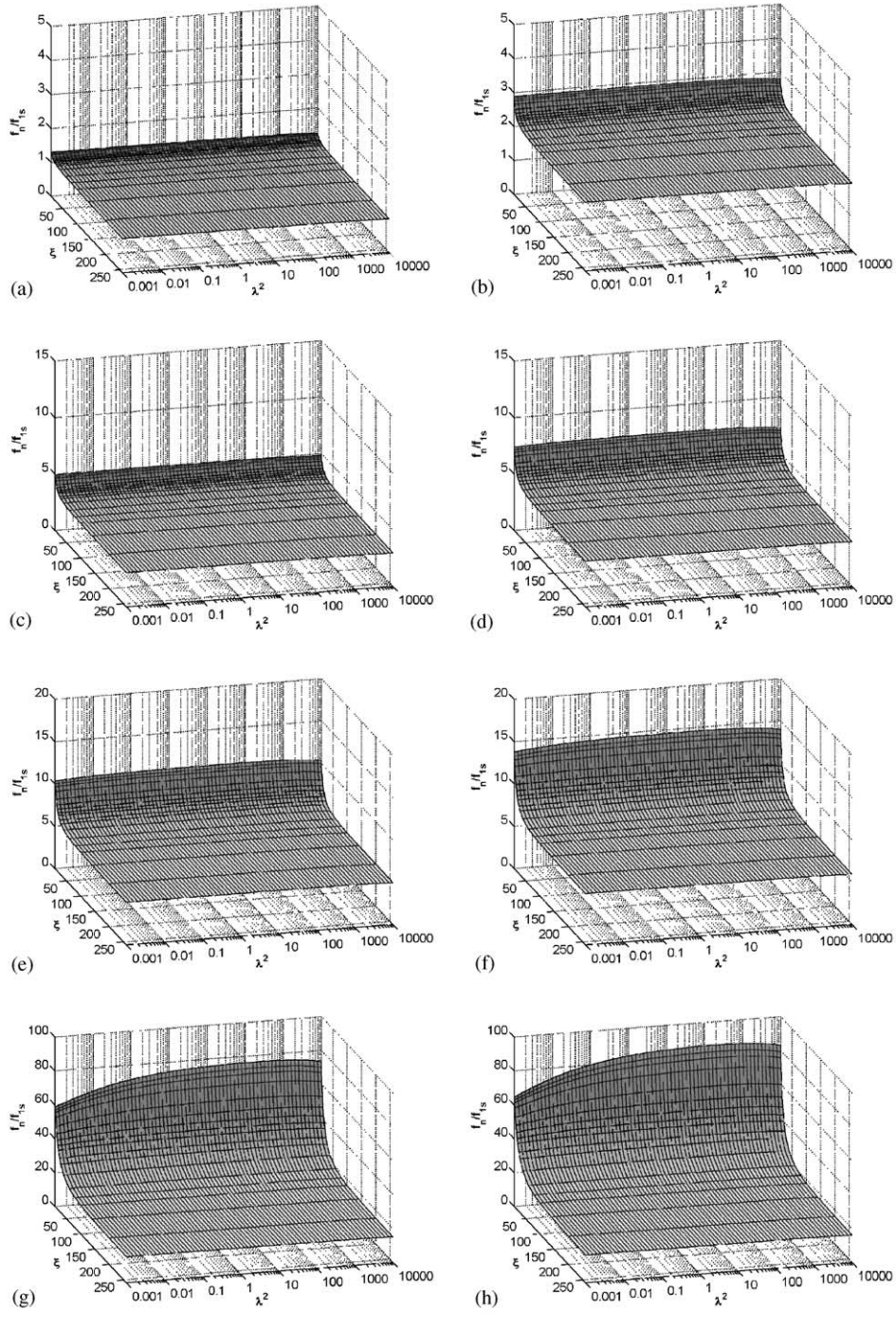

Figure 9. Relation surfaces of out-of-plane modes obtained by the present method for cable set 2: (a) first symmetric mode; (b) first antisymmetric mode; (c) second symmetric mode; (d) second antisymmetric mode; (e) third symmetric mode; (f) third antisymmetric mode; (g) eighth symmetric mode; (h) eighth antisymmetric mode.

4. CASE STUDIES

4.1. TSING MA BRIDGE CABLES

The Tsing Ma Bridge, as shown in Figure 10, is a double deck suspension bridge with a main span of 1377 m and an overall length of 2160 m [1]. The two main cables of the bridge are 36 m apart and have a cross-section of 1.1 m in diameter after compacting. The central span deck and the Ma Wan side span deck are suspended at 18 m intervals by hangers to the main cables. The Tsing Yi side span deck is instead supported from the ground by three concrete piers spaced at 72 m centers. As a result, the main cables on the Tsing Yi side span are free cables without bridge deck being suspended. The modal properties of the Tsing Ma Bridge in different construction stages (including the erection completion stage) have been measured through a series of ambient vibration survey [21]. One stage under measurement is the freely suspended cable stage. In this stage, only the tower–cable system was erected but none of deck segments has been hoisted into position. The main cables on all the three spans were free cables in this stage. The modal parameters of the main cables on the main span and the Tsing Yi side span in this stage are analyzed by the present method and compared with the measurement results for verification. The cable length and sag are 1397·8 and 112·5 m for the suspended main span cable, and 329·1 and 5·7 m for the inclined Tsing Yi side cable. The horizontal component of the tension force is 122 642 kN for both the cables. The main span cable is partitioned into 77 elements and the Tsing Yi side span cable is partitioned into 17 elements. The computation is conducted by assuming the cable supports as pinned ends and fixed ends respectively. Tables 4 and 5 list the natural frequencies of the first three in-plane and out-of-plane modes of the two cables. It is seen that the computed natural frequencies agree favorably with the measurement results.

After completion of the bridge construction, a total of about 300 sensors, including four accelerometers on the main cables, have been permanently installed on the Tsing Ma

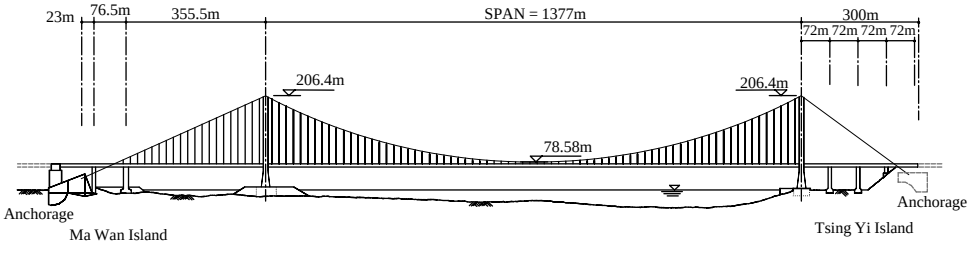

Figure 10. Elevation of Tsing Ma Bridge.

TABLE 4

Natural frequencies of main span cable in freely suspended cable stage (Hz)

Mode no.	Out-of-plane modes			In-plane modes		
	First	Second	Third	First	Second	Third
Computed: pinned ends	0·0522	0·1040	0·1557	0·1008	0·1471	0·2081
Computed: fixed ends	0·0528	0·1052	0·1578	0·1020	0·1488	0·2091
Measurement	0·0530	0·1050	0·1560	0·1020	0·1430	0·2070

TABLE 5

Natural frequencies of Tsing Yi side span cable in freely suspended cable stage (Hz)

Mode no.	Out-of-plane modes			In-plane modes		
	First	Second	Third	First	Second	Third
Computed: pinned ends	0·2352	0·4696	0·7154	0·3527	0·4693	0·7216
Computed: fixed ends	0·2450	0·4946	0·7534	0·3569	0·4943	0·7593
Measurement	0·2360	0·4770	0·7400	0·3430	0·4780	0·7310

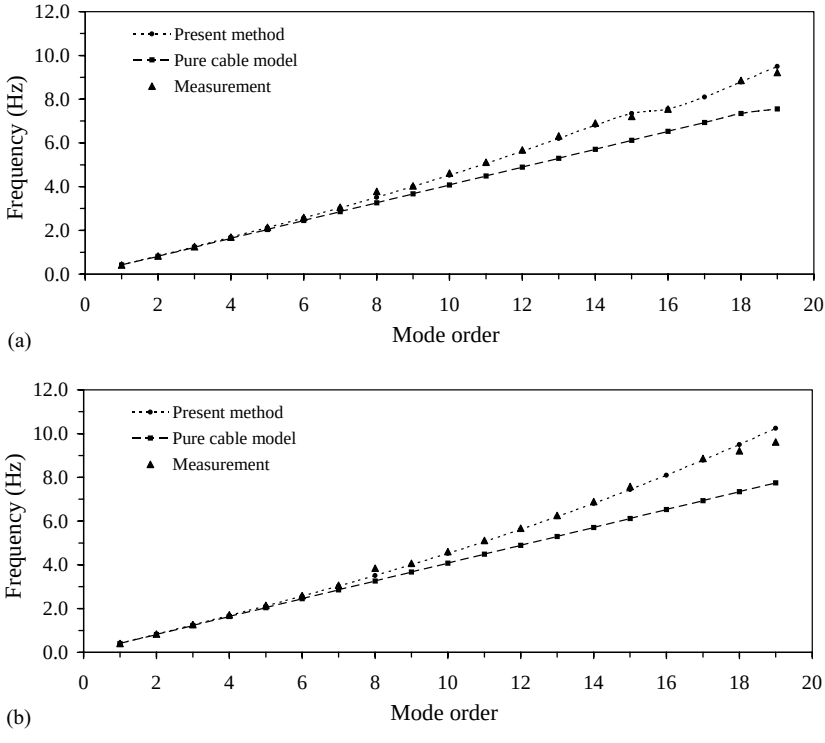

Figure 11. Comparison of computed and measured natural frequencies of Tsing Yi side span cable in erection completion stage: (a) frequencies of in-plane modes; (b) frequencies of out-of-plane modes.

Bridge for structural health and condition monitoring [22]. The tension forces of the Tsing Yi side span free cables can be therefore monitored by means of vibration measurement. In order to examine the effect of cable bending stiffness on the modal properties, the natural frequencies of the Tsing Yi side span free cable in the erection completion stage are predicted using the present method (considering cable bending stiffness) as well as the pure cable model (ignoring cable bending stiffness), and then compared with the measurement results in the same stage from ambient vibration survey. The cable length and sag in this stage are 331·5 and 1·8 m. The horizontal component of the tension force is 405 838 kN. The cable is divided into 200 elements in computation. Figure 11 shows a comparison of the natural frequencies of the first 19 in-plane and out-of-plane modes obtained by the present method, the pure cable model and ambient vibration measurement. Because the

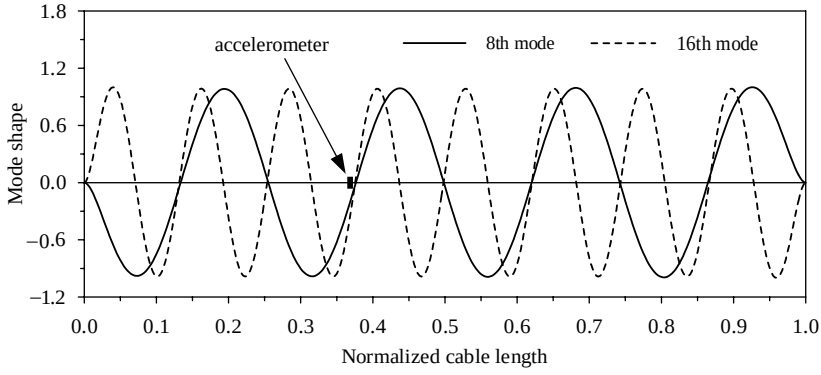

Figure 12. Deployment of accelerometer on cable for ambient vibration measurement.

accelerometer for ambient vibration measurement was located close to a modal node of the eighth and 16th modes as shown in Figure 12, the natural frequencies of these two modes could not be measured with high fidelity. It is observed from Figure 11 that the predicted natural frequencies by the present method agree very well with the measurement results, whereas the natural frequencies predicted using the pure cable model gradually deviate from the measured values with the increase of mode order. The maximum error is as large as 30% for the first 20 modes. This example proves again the significant influence of cable bending stiffness on higher-mode frequencies and the necessity of using an accurate model for multimode-based cable tension and parameter identification.

4.2. TING KAU BRIDGE CABLES

Due to large flexibility, relatively small mass and extremely low damping, structural cables are susceptible to vibration in dynamic conditions. For example, unexpectedly large oscillation occurring in bridge stay cables under specific combinations of wind and rain has been observed in a number of cable-stayed bridges worldwide [23]. This has resulted in increasing application of passive and semi-active dampers in cable-stayed bridges for cable vibration mitigation. For a bridge cable attached with dampers, the existing analytical or approximate formulae are difficult to accurately identify the tension force due to their inability in dealing with damper stiffness effect. The present finite element method does not suffer from this restriction. Modal analysis of the damper-attached Ting Kau bridge cables by the present method is provided here as an example.

As shown in Figure 13, the Ting Kau Bridge is a multi-span cable-stayed bridge with three monoleg towers supporting two main spans of 448 and 475 m and two side spans of 127 m each [8]. In this bridge, eight longitudinal stabilizing cables with a length of up to 465 m have been used to strengthen the slender central tower. Passive dampers have been installed between the cables and deck near the lower ends in the cable planes. The dampers were connected perpendicular to the cables at the location of 19.2 m cable length measured from the lower ends. The length and sag of the longitudinal stabilizing cable are 464·9 m and 8·3 m respectively. The horizontal component of the cable tension force is 2391·5 kN. The cable is divided into 200 elements in computation. Figure 14 illustrates the relation diagrams of the cable natural frequency versus spring (damper) stiffness for the first six in-plane modes. The maximum frequency discrepancy with and without considering damper

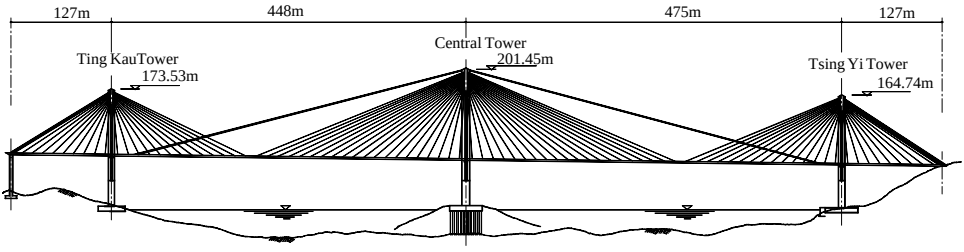

Figure 13. Elevation of Ting Kau Bridge.

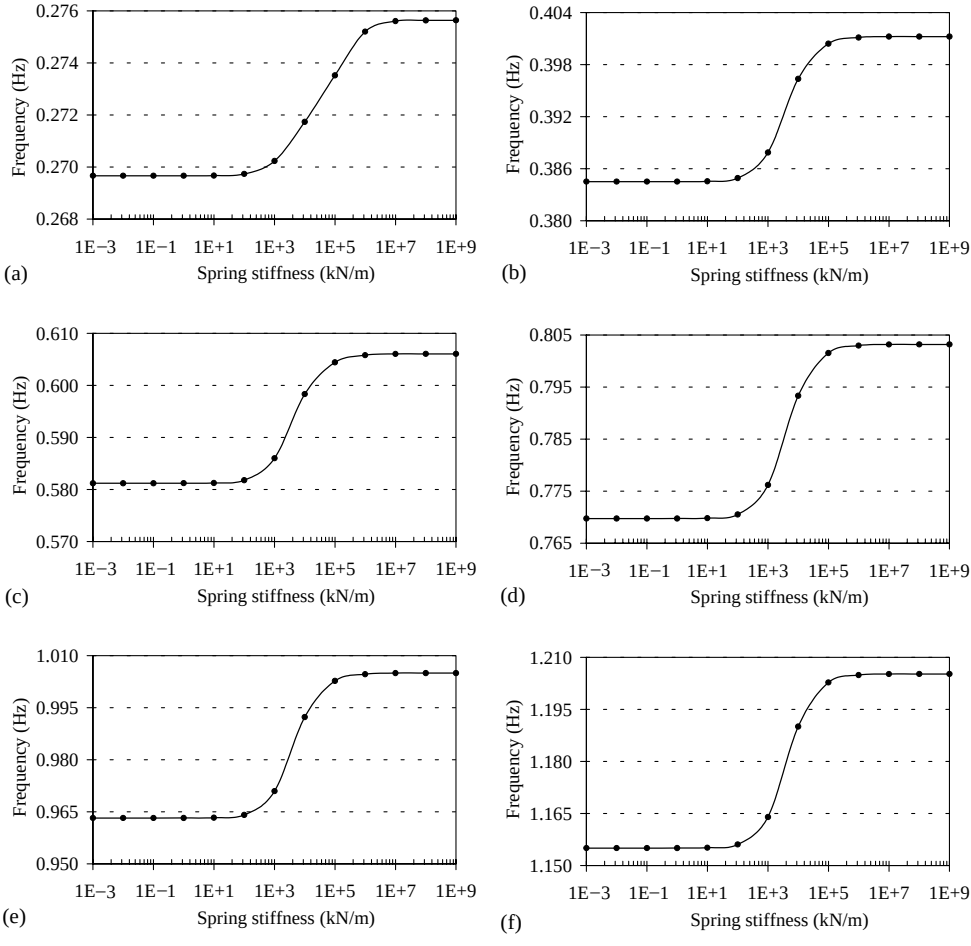

Figure 14. Relation diagrams of natural frequency versus spring (damper) stiffness for Ting Kau bridge stabilizing cable: (a) first mode; (b) second mode; (c) third mode; (d) fourth mode; (e) fifth mode; (f) sixth mode.

stiffness is, respectively, 2·22, 4·35, 4·28, 4·35, 4·34 and 4·35% for the six modes. This means that if each natural frequency of the six modes is used to evaluate tension force from the taut string equation, the maximum identification error of tension force stemming from the damper stiffness effect will be 4·44, 8·70, 8·56, 8·70, 8·68 and 8·70% respectively.

This also demonstrates the importance of a versatile finite element model for tension force evaluation of cables connected with dampers. In addition, it is possible and feasible to simultaneously identify the cable tension force and damper stiffness by use of a precise finite element model and measured multimode frequencies.

5. CONCLUSIONS

In this study a three-dimensional finite element formulation is developed for dynamic analysis of large-diameter structural cables. Only some basic assumptions have been introduced in the finite element modelling and several constraints posed in the conventional cable dynamic analysis have been relaxed in the present study. The proposed formulation is suited for both suspended and inclined cables with arbitrary static profiles, and allows for the consideration of cable flexural rigidity, sag–extensibility, spatial variability of dynamic tension, boundary conditions, lumped masses and intermediate springs and/or dampers. This formulation provides a good baseline model for accurate identification of cable tension force and other structural parameters based on the measurement of multimode frequencies.

Parametric studies are made to evaluate the effect of cable bending stiffness and sag–extensibility on modal properties, and the relation between the natural frequencies and cable parameters for a wide parameter range. The results show that the cable bending stiffness contributes a considerable influence on the natural frequencies when the tension force is relatively small, and affects the higher-mode frequencies more significantly than the lower-mode frequencies. A comparison study of the computed and measured natural frequencies of the Tsing Ma bridge cables shows that taking into account bending stiffness is necessary for large-diameter bridge cables to obtain an accurate prediction of the natural frequencies. The predicted higher-mode frequencies for such cables without considering bending stiffness may significantly deviate from the true values. The case study of the Ting Kau bridge cables demonstrates the effect degree of the stiffness of attached dampers on the cable modal properties and on the tension identification accuracy. It is concluded that the tension forces of long-span large-diameter bridge cables can be accurately evaluated from vibration measurement only when a precise model accounting for cable bending stiffness, sag–extensibility and other constraints is utilized in the identification procedure.

ACKNOWLEDGMENTS

The work described in this paper was supported in part by a grant from the Research Grants Council of the Hong Kong Special Administrative Region, China (Project No. PolyU 5045/00E) and partially by a grant from the Hong Kong Polytechnic University (Project No. G-V785).

REFERENCES

1. A. S. Beard 1995 *Structural Engineering International* **5**, 138–140. Tsing Ma Bridge, Hong Kong.
2. S. Saeki, Y. Fujino, K. Tada, M. Kitagawa and T. Kanazaki 1995 in *Restructuring: America and Beyond* (M. Sanayei, editor), 237–252. New York: American Society of Civil Engineers. Technological aspects of the Akashi Kaikyo Bridge.

3. K. K. Ng, H. C. Wong, C. H. Hui and K. P. Wong 2000 in *Civil Engineering in the 21st Century* (J. Song and G. Zhou, editors), 596–603. Beijing: Science Press. Stonecutters Bridge design competition.
4. M. C. H. Hui 2001 in Proceedings of the 10th National Symposium on Structural Wind Engineering, Guilin, China, 84–93. Stonecutters Bridge—deck section optimization.
5. M. Ito and T. Endo 1994 in *Structures Congress XII* (N. C. Baker and B. J. Goodno, editors), 677–682. New York: American Society of Civil Engineers. The Tatara Bridge—world's longest cable–stayed span.
6. M.-C. Tang 1995 in *Restructuring: America and Beyond* (M. Sanayei, editor), 455–458. New York: American Society of Civil Engineers. Multispan cable-stayed bridges.
7. M. Virlogeux 2001 *Structural Engineering International* **11**, 61–82. Bridges with multiple cable-stayed spans.
8. R. Bergermann and M. Schlaich 1996 *Structural Engineering International* **6**, 152–154. Ting Kau Bridge, Hong Kong.
9. K. J. Kroneberger-Stanton and B. R. Hartsough 1992 *Transactions of the ASAE* **35**, 341–346. A monitor for indirect measurement of cable vibration frequency and tension.
10. J. R. Casas 1994 *Structural Engineering International* **4**, 235–240. A combined method for measuring cable forces: the cable-stayed Alamillo Bridge, Spain.
11. J. C. Russell and T. J. Lardner 1998 *American Society of Civil Engineers Journal of Engineering Mechanics* **124**, 1067–1072. Experimental determination of frequencies and tension for elastic cables.
12. A. Cunha and E. Caetano 1999 *Experimental Techniques* **23**, 38–43. Dynamic measurements on stay cables of cable-stayed bridges using an interferometry laser system.
13. H. Zui, T. Shinke and Y. Namita 1996 *American Society of Civil Engineers Journal of Structural Engineering* **122**, 651–656. Practical formulas for estimation of cable tension by vibration method.
14. W.-H. P. Yen, A. B. Mehrabi and H. Tabatabai 1997 in *Building to Last* (L. Kempner Jr and C. B. Brown, editors), 503–507. New York: American Society of Civil Engineers. Evaluation of stay cable tension using a non-destructive vibration technique.
15. A. B. Mehrabi and H. Tabatabai 1998 *American Society of Civil Engineers Journal of Structural Engineering* **124**, 1313–1322. Unified finite difference formulation for free vibration of cables.
16. G. Zheng, J. M. Ko and Y. Q. Ni 2001 in *Smart Structures and Materials 2001: Smart Systems for Bridges, Structures, and Highways* (S. C. Liu, editor), *Proceedings of SPIE*, Vol. 4330, 511–522. Bellingham: The International Society for Optical Engineering. Multimode-based evaluation of cable tension force in cable-supported bridges.
17. M. S. Triantafyllou 1984 *Shock and Vibration Digest* **16**, 9–17. Linear dynamics of cables and chains.
18. H. M. Irvine 1981 *Cable Structures*. Cambridge: The MIT Press.
19. U. Starossek 1994 *Structural Engineering International* **4**, 171–176. Cable dynamics—a review.
20. J. M. Ko, G. Zheng and Y. Q. Ni 2000 in *Proceedings of the International Conference on Advanced Problems in Vibration Theory and Applications, Xi'an, China*, 437–443. Periodically forced vibration of nonlinear stay cables.
21. J. M. Ko, Y. Q. Ni and J. Y. Wang 2000 in *Proceedings of the International Conference on Advanced Problems in Vibration Theory and Applications, Xi'an, China*, 285–291. Tsing Ma suspension bridge: ambient vibration survey campaigns.
22. C. K. Lau, W. P. N. Mak, K. Y. Wong, W. Y. K. Chan and K. L. D. Man 1999 in *Structural Health Monitoring 2000* (F.-K. Chang, editor), 450–460. Lancaster: Technomic Publishing Corporation. Structural health monitoring of three cable-supported bridges in Hong Kong.
23. R. W. Poston 1998 *American Society of Civil Engineers Civil Engineering* **68**, 58–61. Cable-stay conundrum.